EMT three-phase VSC grid-connected converter reactive power control using H∞ LMI MIMO approach

Hoang-Trung Ngo, Elkhatib Kamal, Bogdan Marinescu

EMT three-phase VSC grid-connected converter reactive power control using H_∞ LMI MIMO approach

Hoang-Trung NGO, Elkhatib KAMAL, Bogdan MARINESCU

***Abstract*—With the increasingly rapid penetration of power electronics into AC grid, there is an urgent need in enhancing stability and performance of grid-connected converters. An advanced H_∞ multi-input multi-output (MIMO) control using linear matrix inequality (LMI) techniques is introduced and applied for electromagnetic transient (EMT) three-phase voltage source converter (VSC) grid-connected system (simple STATCOM). The proposed control is compared with classical cascade vector control through a validation test of short-circuit event.**

The comparison results prove that the advanced control approach provides much better performance and transient behaviour compared to classic vector controls, as a result of using H_∞ optimization technique to minimize the effect of frequency's and grid voltage's variations.

The validation test is done using MATLAB Simscape in EMT simulation, and also gives a step-by-step path of implementation for applying advanced control in industrial-level application of power converter.

These results will be further used to control the units of the new concept of *Dynamic Virtual Power Plant* introduced in the H2020 POSYTYF project.

***Index Terms*—EMT, VSC, LMI, H-infinity, MIMO, disturbance rejection, STATCOM**

I. Introduction

VOLTAGE Source Converters (VSC) are used to link AC and DC systems employing high-power electrical devices like IGBTs. VSCs can self-commutate, which means they can create AC voltages without the need of an AC system, enabling independent, quick control of active and reactive power, as well as black start capabilities. As a result, VSC is rapidly adopted for transmission system [1] (e.g. HVDC and Flexible AC Transmission (FACT)) and in converter-based generators [2](e.g. wind energy systems).

In particular, the widespread VSC-based FACT applications such as Static Synchronous Compensator (STATCOM), preferred over old technology like Static var compensators (SVC), are intensively studied [3]. An SVC contribute AC voltage service using dynamic reactive power regulation by means of thyristor-controlled reactors (TCR) and thyristor-switched capacitors (TSC) for Var absorption and production respectively. A STATCOM achieves the same result by synthesizing a voltage waveform of variable magnitude with respect to the system voltage using a VSC. In addition, STATCOM is controlled with Pulse Width Modulation (PWM) and allows thus faster response and thereby markedly improves power quality [3].

Recently, there are many studies conducted for improving the VSC produced power quality, including cascade control (i.e., classical vector control) [4] and advanced Multi-Input Multi-Output (MIMO) control [5] [6]. The two-loops cascade control approach use feed-forward decoupling terms to separate the two d-axis current and q-axis current [4]. This is less efficient than advanced optimal H_∞ disturbance rejection techniques such as [5]. As proven in these works (e.g., in our previous work [5]), the new MIMO control methodology provides much better performance and stability margin.

However, there are still very few works on advanced control which are validated in Electromagnetic Transients (EMT) simulation to prove the applicability of new approach for industrial-level implementation. This paper presents an EMT validation test for VSC grid-connected reactive power control (a simple version of STATCOM), using both of classical cascade control and advanced H_∞ control (using Linear Matrix Inequality (LMI)). By comparing the two control approaches, the paper provides a practical look into their advantages and disadvantages. Simultaneously, the advanced MIMO control is validated and proven to be applicable for industrial applications.

The paper is organized as follows. Section II provides the VSC EMT model (in abc-frame and dq-frame) using MATLAB/Simscape, and cascade vector control approach is also presented. Next, in Section III, the MIMO H_∞ LMI approach will be introduced. The validation tests and their results are be presented in Section IV. Finally, the conclusions will be formulated in Section V.

II. EMT model of VSC grid-connected converter

A. VSC grid-connected converter reactive power control - Simple STATCOM

As discussed, in this section, the EMT model of VSC grid-connected converter for STATCOM application is presented.

Hoang-Trung NGO, Elkhatib KAMAL and Bogdan MARINESCU are with Ecole Centrale Nantes -LS2N (Laboratoire des sciences du numérique de Nantes), 1 Rue de la Noë, 44000 Nantes Cedex 3, France, Email: Bogdan.Marinescu@ec-nantes.fr, Elkhatib.Ibrahim@ec-nantes.fr and Hoang-Trung.Ngo@ec-nantes.fr.

This project has received funding from the European Union's Horizon 2020 research and innovation programme under grant agreement No. 883985 (POSYTYF – POwering SYstem flexibiliTY in the Future through RES, https://posytyf-h2020.eu/)

978-1-6654-8032-1/22/$31.00 ©2022 IEEE

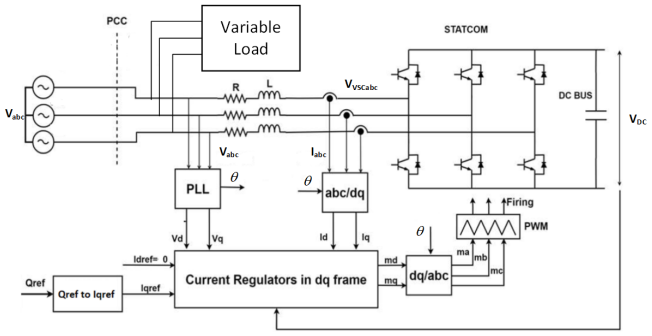

Fig. 1. VSC grid-connected reactive power control - simple STATCOM

Variable	Detailed information	value	unit
V_{grid}	RMS phase-phase voltage of AC grid	400	V
V_{DC}	DC voltage value of VSC	1000	V
f_s	Switching frequency of VSC	5000	Hz
f	Voltage frequency of the AC system	50	Hz
T_s	Sample time for EMT simulation	10	μs
R	R value of transmission line	0.02	Ω
L	L value of transmission line	0.01	H
R_1	R value of R-L load 1	2	Ω
L_1	L value of R-L load 1	0.02	H
R_2	R value of R-C load 2	2	Ω
C_2	C value of R-C load 2	0.02	F

TABLE I
THE DATA FOR EMT VSC GRID-CONNECTED MODEL IN SIMSCAPE

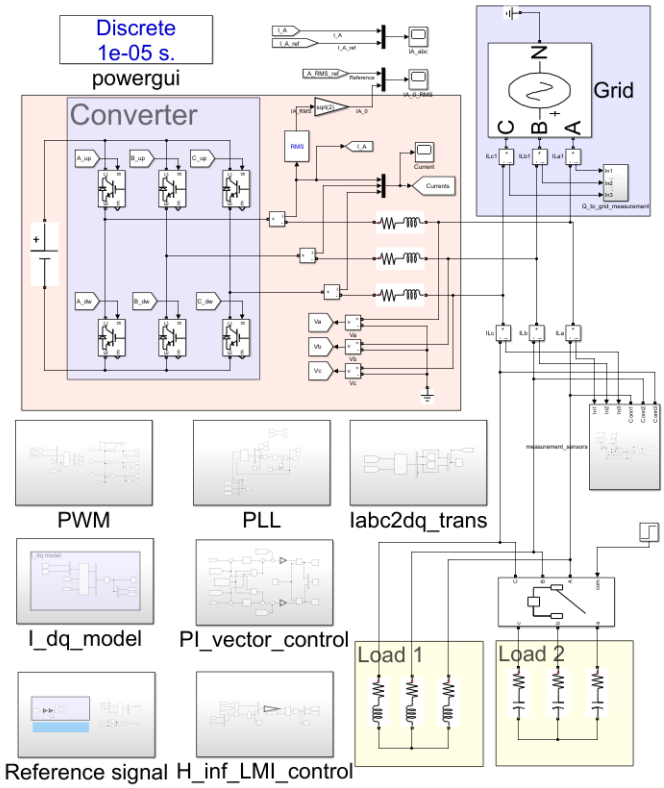

Fig. 2. EMT VSC grid-connected reactive power control using Simscape

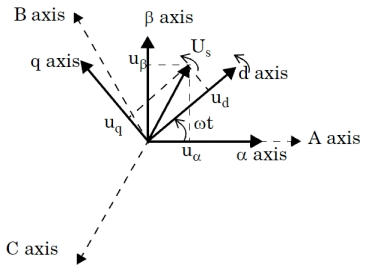

Fig. 3. abc and dq frame in Park transformation

The VSC in this application is a 3-phase 2-level VSC, used for compensating reactive power for the load (see Fig. 1). The classical cascade control is also presented in this Section, while the proposed advanced MIMO control is presented in the next Section (Section III).

The VSC grid-connected converter model is presented in Fig. 1. It consists of a three-phase two-level VSC, connected to grid V_{abc} through a transmission line (a R-L line equivalence is used). A variable load is also connected to the Point of Common Coupling (PCC). The Phase Locked Loop (PLL) is to create the phase angle θ of grid voltage, which then is used to calculate currents in dq frame I_{dq} from three-phase currents I_{abc}. The phase angle θ is also used to convert the control signal in dq frame m_{dq} to control signal in abc frame m_{abc}, which then produces firing signal to control the converter.

To act as a STATCOM, the converter has to be able to produce the same amount reactive power required by the variable load, i.e. ensuring the reactive power flow to grid at PCC equal to zero. The active power is also kept as zero value. The EMT model will be presented in the next subsection (subsection II-B), and these objectives are then translated into control objectives in subsection II-C.

B. Electromagnetic transient model

The VSC grid-connected converter model from subsection II-A (Fig. 1) is now implemented in EMT model using MATLAB/Simulink Simscape as in Fig. 2. The 2-level VSC is built using 6 IGBT (or GTO or MOSFET)/Diode pair where the forward voltages of the forced-commutated device. The power source of VSC is a DC voltage source. The transmission line between VSC and AC grid is modeled by equivalent three-phase RL branch. For the variable load, two R-L load and R-C load are used. The AC grid side is modeled using three-phase voltage source. The data for the EMT is shown in Table I.

C. System modelling in abc/dq frames and control objectives

The voltage V_{VSCabc} at terminal of VSC are in sine-wave form, in which it is very hard to implement internal model principle control [8] for reference tracking. Instead of control ling voltage in abc frame, the controller can control voltage in dq frame which are rotating which the same speed $\theta = \omega t$ as of voltage in abc frame [4] as in Fig. 3. The system equation in abc frame is (1).

$$\frac{dI_{abc}}{dt} = \frac{1}{L}\left(-RI_{abc} - V_{abc} + V_{VSCabc}\right) \quad (1)$$

where $I_{abc} = \begin{bmatrix} i_a & i_b & i_c \end{bmatrix}^T$, $V_{abc} = \begin{bmatrix} V_a & V_b & V_c \end{bmatrix}^T$ and $V_{VSCabc} = \begin{bmatrix} V_{VSCa} & V_{VSCb} & V_{VSCc} \end{bmatrix}^T$.

The inverse Park transform (as in Fig. 3) from abc frame to dq frame ($\theta = \omega t$):

$$I_{abc} = TI_{dq0}; V_{abc} = TV_{dq0}; V_{VSCabc} = TV_{VSCdq0} \quad (2)$$

where $I_{dq0} = \begin{bmatrix} i_d & i_q & i_0 \end{bmatrix}^T$, $V_{abc} = \begin{bmatrix} V_d & V_q & V_0 \end{bmatrix}^T$ and $V_{VSCdq0} = \begin{bmatrix} V_{VSCd} & V_{VSCq} & V_{VSC0} \end{bmatrix}^T$

and the transform matrix is

$$T = T(\theta) = \begin{bmatrix} \cos\theta & -\sin\theta & 1 \\ \cos\left(\theta - \frac{2\pi}{3}\right) & -\sin\left(\theta - \frac{2\pi}{3}\right) & 1 \\ \cos\left(\theta + \frac{2\pi}{3}\right) & -\sin\left(\theta + \frac{2\pi}{3}\right) & 1 \end{bmatrix} \quad (3)$$

Equation (1) becomes

$$\frac{d\left[TI_{dq0}\right]}{dt} = \frac{1}{L}\left(-RTI_{dq0} - TV_{dq0} + TV_{VSCdq0}\right) \quad (4)$$

Since $\frac{d[TI_{dq0}]}{dt} = \frac{dT}{dt}I_{dq0} + T\frac{dI_{dq0}}{dt}$, equation (4) is equivalent to:

$$T^{-1}\frac{dT}{dt}I_{dq0} + \frac{dI_{dq0}}{dt} = \frac{1}{L}\left(-RI_{dq0} - V_{dq0} + V_{VSCdq0}\right) \quad (5)$$

In addition, we have:

$$T^{-1}\frac{dT}{dt} = X_T = \begin{bmatrix} 0 & -\dot{\theta} & 0 \\ \dot{\theta} & 0 & 0 \\ 0 & 0 & 0 \end{bmatrix} \quad (6)$$

The system equation in dq frame (5) are now:

$$X_T I_{dq0} + \frac{dI_{dq0}}{dt} = \frac{1}{L}\left(-RI_{dq0} - V_{dq0} + V_{VSCdq0}\right) \quad (7)$$

Do notice that voltage in abc frame are balanced, i.e. $V_a + V_b + V_c = 0$, therefore in qd frame, we have $V_0 = 0$ and $i_0 = 0$. Also, based on averaged model [4], the VSC terminal voltage in dq frame are (where $m_0 = 0$ since $V_0 = 0$):

$$V_{VSCdq0} = \frac{V_{DC}}{2}\begin{bmatrix} m_d & m_q & m_0 \end{bmatrix}^T \quad (8)$$

By using PLL (Fig. 1) with d-axis aligned with a-axis (Fig. 3), voltage is imposed with $V_q = 0$. Thus, the output powers at PCC in dq frame [4]:

$$\begin{cases} P = \frac{3}{2}\left(V_d i_d + V_q i_q\right) = \frac{3}{2}V_d i_d \\ Q = \frac{3}{2}\left(-V_d i_q + V_q i_d\right) = -\frac{3}{2}V_d i_q \end{cases} \quad (9)$$

The reference for current control from power reference signal P_{ref}, Q_{ref} are:

$$\begin{cases} I_{dref} = \frac{2}{3}\frac{P_{ref}}{V_d} \\ I_{qref} = -\frac{2}{3}\frac{Q_{ref}}{V_d} \end{cases} \quad (10)$$

As discussed in subsection II-A, to act as a STATCOM, the converter must compensate the reactive power required from loads and produce no active power, i.e. the power reference signals are $P_{dref} = 0$ and $Q_{qref} = -Q_{load}$. The control objectives are then translated into current reference signals as:

$$\begin{cases} I_{dref} = 0 \\ I_{qref} = \frac{2}{3}\frac{Q_{load}}{V_d} \end{cases} \quad (11)$$

D. Cascade vector control

As a general rule, the classical vector control considers grid frequency ω as a constant (i.e. $\dot{\theta} = \omega$, $\omega = \omega_0 = 100\pi$) [4]. As a result, the dq system equation in (7) becomes:

$$\begin{cases} \frac{di_d}{dt} = -\frac{R}{L}i_d + \omega_0 i_q + \frac{1}{L}\left(-V_d + \frac{m_d V_{DC}}{2}\right) \\ \frac{di_q}{dt} = -\frac{R}{L}i_q - \omega_0 i_d + \frac{1}{L}\left(-V_q + \frac{m_q V_{DC}}{2}\right) \end{cases} \quad (12)$$

where m_d and m_q are control signal as in Fig. 1.

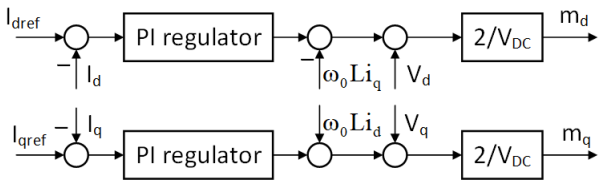

Fig. 4. the cascade current control using decoupling terms

The classical control using two separated PI control loops [4] presented as in Fig. 4. To decouple the current in dq frame (equation (12)), the feed-forward decoupling terms $\{\omega L i_q, V_d\}$ (for i_d control) and $\{\omega L i_d, V_q\}$ (for i_q control) are used. This control structure with feed-forward method helps to reduce the transient overshoot/undershoot, but is far from optimal compared to advanced MIMO control techniques (which can be seen in Section IV).

The two i_d and i_q dynamics are handled by identical PI control, with closed-loop transfer function (from i_{ref} to i for both of i_d and i_q dynamics) are:

$$i(s) = i_{ref}(s)\frac{G(s)}{1 + G(s)}; G(s) = \frac{K_P}{Ls}\frac{s + \frac{K_i}{K_p}}{s + \frac{R}{L}}$$

Using pole cancellation for the pole of $s + \frac{R}{L}$, i.e. set $\frac{K_i}{K_p} = \frac{R}{L}$, the closed-loop becomes:

$$i(s) = i_{ref}(s)\frac{1}{1 + \frac{L}{K_P}s}$$

The gain K_p and K_i are then defined by choosing the suitable time constant $\tau_i = \frac{L}{K_P}$ for this closed-loop, i.e. $K_P = \frac{L}{\tau_i}$ and $K_i = K_p\frac{R}{L} = \frac{R}{\tau_i}$.

III. H_∞ LMI MIMO CONTROL SYNTHESIS

To obtain a controller with optimal performance, MIMO control structure using state-space method is used. The non-linear model (12) is linearized at chosen operating point, then the controller will be synthesized based on obtained linear model. The LMI conditions can be constructed and modified based on requirement of the designer (e.g. pole placement, H_∞ optimization and/or minimum gain). In this paper, the proposed control is constructed using pole placement and H_∞ optimization, but other LMI conditions can be easily added to the overall condition to meet the need of control design.

A. Augmented system for MIMO control design

Consider the operating point of nonlinear model (12):

$$\begin{bmatrix} i_d^* \\ i_q^* \end{bmatrix} = \begin{bmatrix} i_{d0} \\ i_{q0} \end{bmatrix}; \begin{bmatrix} m_d^* \\ m_q^* \end{bmatrix} = \begin{bmatrix} m_{d0} \\ m_{q0} \end{bmatrix} \tag{13}$$

The classical vector control considers $\omega = \omega_0 = 100\pi$ and grid voltage V_{abc} are constant (i.e. $\Delta V_d = 0$ and $\Delta V_q = 0$ in equation (14)). This is not totally true in practice. Therefore, to improve performance, a *disturbance rejection* will be ensured in control synthesis in order to minimize the effect of frequency and grid voltage variations.

When taking into account the variations of grid frequency and voltage variations (and still considering the averaged model of VSC terminal voltage in (8)), the linearized model version of nonlinear model (7) is (where $\omega_0 = 100\pi$ is the nominal frequency):

$$\begin{cases} \frac{d\Delta i_d}{dt} = -\frac{R}{L}\Delta i_d + \omega_0\left(\frac{\dot\theta}{\omega_0}\Delta i_q + i_q\frac{\Delta\dot\theta}{\omega_0} + \frac{-\Delta V_d}{\omega_0 L}\right) + \frac{V_{DC}}{2L}\Delta m_d \\ \frac{d\Delta i_q}{dt} = -\frac{R}{L}\Delta i_q - \omega_0\left(\frac{\dot\theta}{\omega_0}\Delta i_d + i_d\frac{\Delta\dot\theta}{\omega_0} + \frac{\Delta V_q}{\omega_0 L}\right) + \frac{V_{DC}}{2L}\Delta m_q \end{cases} \tag{14}$$

The model (14) is written in state-space form with state X, control signal U and disturbance W:

$$\begin{cases} \dot X = AX + B_1U + B_2W \\ Y = X \end{cases} \tag{15}$$

where:

$$X = \begin{bmatrix} \Delta i_d \\ \Delta i_q \end{bmatrix} = \begin{bmatrix} i_d \\ i_q \end{bmatrix} - \begin{bmatrix} i_{d0} \\ i_{q0} \end{bmatrix};$$
$$U = \begin{bmatrix} \Delta m_d \\ \Delta m_q \end{bmatrix} = \begin{bmatrix} m_d \\ m_q \end{bmatrix} - \begin{bmatrix} m_{d0} \\ m_{q0} \end{bmatrix};$$
$$W = \begin{bmatrix} \frac{\dot\theta}{\omega_0}\Delta i_q + i_q\frac{\Delta\dot\theta}{\omega_0} + \frac{-\Delta V_d}{\omega_0 L} \\ \frac{\dot\theta}{\omega_0}\Delta i_d + i_d\frac{\Delta\dot\theta}{\omega_0} + \frac{\Delta V_q}{\omega_0 L} \end{bmatrix}$$

and state-space matrices are:

$$A = \begin{bmatrix} -\frac{R}{L} & 0 \\ 0 & -\frac{R}{L} \end{bmatrix}; B_1 = \begin{bmatrix} \frac{V_{DC}}{2L} & 0 \\ 0 & \frac{V_{DC}}{2L} \end{bmatrix}; B_2 = \begin{bmatrix} \omega_0 & 0 \\ 0 & -\omega_0 \end{bmatrix}$$

The objective is to ensure output reference asymptotic tracking: $e = -Y + Y_{ref} = -X + Y_{ref} \to 0$, where $Y_{ref} = \begin{bmatrix} i_{dref} & i_{qref} \end{bmatrix}^T$ (see equation (11)).

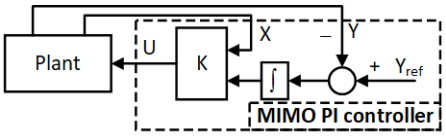

Fig. 5. The MIMO PI controller implementation

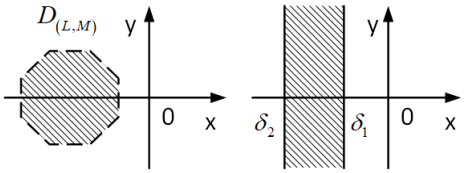

Fig. 6. The general LMI region $D_{(L,M)}$ (left) and strip region (right)

To achieve this, internal model principle [8] is used to produce an *augmented state system* starting from the physical system (15):

$$\begin{cases} \dot{\bar X} = \bar A\bar X + \bar B_1\bar U + \bar B_2\bar W \\ \bar Y = e = \bar C\bar X \end{cases} \tag{16}$$

where:

$$\bar X = \begin{bmatrix} \dot X \\ e \end{bmatrix}; \bar U = \dot U; \bar W = \dot W$$

and the augmented matrices are:

$$\bar A = \begin{bmatrix} A & 0 \\ -I & 0 \end{bmatrix}; \bar B_1 = \begin{bmatrix} B_1 \\ 0 \end{bmatrix}; \bar B_2 = \begin{bmatrix} B_2 \\ 0 \end{bmatrix}; \bar C = \begin{bmatrix} 0 \\ I \end{bmatrix}^T$$

The state-feedback controller of augmented system (16) is $\bar U = K\bar X$. The MIMO PI controller of system (15) can now be recovered as:

$$\begin{cases} U = \begin{bmatrix} \Delta m_d \\ \Delta m_q \end{bmatrix} = K\begin{bmatrix} X \\ \int e dt \end{bmatrix} \\ \begin{bmatrix} m_d \\ m_q \end{bmatrix} = U + \begin{bmatrix} m_{d0} \\ m_{q0} \end{bmatrix} \end{cases} \tag{17}$$

The MIMO PI control (17) can be easily implemented as in Fig. 5 (using abc-dq control structure in Fig. 1), where the plant is the original system in dq frame (12).

B. Pole-placement LMI techniques

To obtain the gain K (as in (17)) with suitable closed-loop characteristics (e.g. same time constant as vector control in subsection II-D), the closed-loop poles should be limited into a region on the complex plane.

Consider symmetric matrix L and square matrix M, the general LMI region is defined as [9]:

$$D_{(L,M)} = \left\{ s \,\middle|\, s \in C, L + sM + \bar s M^T < 0 \right\} \tag{18}$$

Described in Fig. 6, the LMI region $D_{(L,M)}$ is convex and symmetric about the real axis [9].

For limiting the closed-loop time constant $\tau_{closed-loop}$ in a comparable range compared to vector control's time constant, i.e. $-\frac{1}{\delta_2} < \tau_{closed-loop} < -\frac{1}{\delta_1}$. Equivalently, the closed-loop poles will be limited in a range $\delta_2 < s < \delta_1$, which is a strip region as in Fig. 6. The strip region is a special case of general LMI region $D_{(L,M)}$ with:

$$L = \begin{bmatrix} -2\delta_2 & 0 \\ 0 & 2\delta_1 \end{bmatrix}; M = \begin{bmatrix} 1 & 0 \\ 0 & -1 \end{bmatrix} \tag{19}$$

C. H_∞ LMI MIMO control with pole placement condition

To find the gain K for augmented system (16) with closed-loop pole belong to the LMI region $D_{(L,M)}$ (equation (18)), the H_∞ problem is introduced and its theorem is proposed as follows.

Problem 1: For the linear system (16), the H_∞ problem is to design a state feedback control law $\bar{U} = K\bar{X}$ such that:

$$\|G(s)\|_\infty \leq \gamma \tag{20}$$

hold for a given positive scalar γ (where $G(s) = \frac{\bar{Y}(s)}{\bar{W}(s)}$).

Theorem 1:

The mentioned H-infinity problem 1 has a solution if and only if there exist a matrix W_P and a symmetric positive definite matrix X_P , through the LMI-based minimization such that

$$\underset{X_P, W_P}{minimize} \quad \gamma$$

subject to

$$\begin{cases} \begin{bmatrix} \Psi & \bar{B}_2 & \left(\bar{C}X_p\right)^T \\ \bar{B}_2^T & -\gamma I & 0 \\ \bar{C}X_p & 0 & -\gamma I \end{bmatrix} < 0 \\ L \otimes X_P + M \otimes \Psi_1 + M^T \otimes \Psi_1^T < 0 \\ \Psi = \Psi_1 + \Psi_1^T; \Psi_1 = \bar{A}X_P + \bar{B}_1 W_P \end{cases}$$

where $\otimes$ is Kronecker product.

The matrix gain K can be recovered as:

$$K = W_P X_P^{-1} \tag{21}$$

Proof 1:

The proof for H_∞ optimization (first LMI condition) can be seen in [9] in general linear system and in [5], [6] for VSC-based systems. The proof for pole placement (second LMI condition) can be seen in [9].

IV. Simulations and results

In this Section, the validation tests of proposed control are run with the EMT model in Fig. 2 using MATLAB Simscape. The results are also compared with the ones obtained in the same test conditions with the classical cascade vector control presented in subsection II-D.

The validating scenario is as in Fig. 1, but with R-L load 1 connected to the VSC and the AC grid (RC- load 2 is disconnected). At t = 1s a balanced short-circuit (as in Fig. 7) is considered at the middle of the transmission line (R-L line). The parameters of short-circuit fault are $R_{on} = 0.1\Omega$ and $R_g = 0.01\Omega$. The fault clears at t = 1.1s.

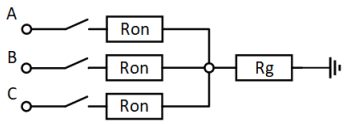

Fig. 7. Three-phase fault implementation

The two controller methods (H_∞ LMI MIMO and cascade vector control) using the same structure as in Fig. 1, with the PLL a standard PI control with proportional gain 213, integral gain 49348 and with back-calculation anti-windup.

For classical cascade vector control, the PI controllers are tuned with time constant $\tau_i = 2ms$ (10 times of switching period $\tau_s = \frac{1}{f_s} = 0.2ms$). The PI control gains in the two loops are identical: $K_p = 5$ and $K_i = 10$.

In the case of MIMO current control mentioned in Section II using proposed control (Section III), the pole placement condition is only for time constant of closed-loop, i.e. the LMI pole placement condition is with matrices L and M in (19). The LMI condtions are then written in MATLAB using YALMIP toolbox [10], and is solved by MOSEK solver [11]. The closed-loop time constant for both of i_d and i_q are $\tau_i^* = 2.19ms$ (close to $\tau_i = 2ms$ of vector control). The gain K of MIMO PI control are small and comparable to vector control's gain:

$$K = \begin{bmatrix} -0.025 & 0 & 7.278 & 0 \\ 0 & -0.025 & 0 & 7.278 \end{bmatrix}$$

To act as a STATCOM, the main role of VSC is to keep acive power flow to grid from PCC at zero, as illustrated in Fig. 8. Before and after the short-circuit event, the perfomance of proposed control is superior to those of classical control. Indeed, the chattering range is only around 60% compared to the wider chattering range obtained for the classical control. Also, duration of the transient is around 10ms while the classical vector control needs 20ms. This is due to the superior performance in current control using H_∞ LMI MIMO, which will be explain in the following paragraph.

The responses of the VSC AC terminal current (phase A only, since abc phases are balanced) obtained with both classical vector control and H_∞ LMI control are presented in Figs. 9, 10 and 11. In steady-state operation, i.e., before the short-circuit, the proposed control provides lower level chattering around the reference values considerably compared to the classical vector control as shown in Fig. 10. This is also clearly seen in Root Mean Square (RMS) representation of phase A current in Fig. 12, where the chattering amplitude of classical control is at least as double as the one of proposed control. This is due to the global improvement of the performances observed also in Fig. 13 in dq frame. Also, as shown in Figs. 12 and 13, during and after the short-circuit event, the performances of proposed control are significantly superior to vector control ones. The duration of the transients with

advanced current control is much smaller than the one obtained with vector control (5ms compared to nearly 800ms). Also, overshoots and undershoots of the current are 2 times smaller in dq frame and 5 times smaller for RMS measurements.

V. Conclusions

In this paper, an advanced control using H_∞ optimization based on LMI techniques is proposed and validated in EMT three-phased VSC grid-connected system. The proposed approach is also compared to vector control in terms of performance and transient behaviour.

The proposed control provides better better control performances, transient behaviour and quality of powers, thanks to its disturbance rejection using H_{inf} optimization to minimize the effect of grid frequency and grid voltage variations. The paper also demonstrates the proposed control's applicability and step-by-step guide for implementing the advanced MIMO control in VSC-based industrial-level application.

The proposed approach will be used to implement a multi-objective control structure for POSYTYF project in the near future. Also, hardware in the loop validation will follow.

References

[1] ENTSOE, TYNDP 2018 (2019, October), Technologies for Transmission System.

[2] Vormedal, P. K. M. (2010). Voltage Source Converter Technology for Offshore Grids. Norwegian University of Science and technology, Trondheim, Master thesis.

[3] Bahrman, M. P., Johansson, J. G., & Nilsson, B. A. (2003, July). Voltage source converter transmission technologies: the right fit for the application. In 2003 IEEE Power Engineering Society General Meeting (IEEE Cat. No. 03CH37491) (Vol. 3, pp. 1840-1847). IEEE.

[4] Bacha, S., Munteanu, I., & Bratcu, A. I. (2014). Power electronic converters modeling and control. Advanced textbooks in control and signal processing, 454(454).

[5] Marinescu, B., Kamal, E., & Ngo, H. T. (2021). A System Model-Based Approach for the Control of Power Park Modules for Grid Voltage and Frequency Services. arXiv preprint arXiv:2107.02000.

[6] Ngo, H. T., Kamal, E., Marinescu, B., & Xavier, F. (2020, November). Robust H_∞ Decentralized Control Design for HVDC Link Embedded in a Large-scale AC Grid. In 2020 Electrical Power and Energy Conference.

[7] Singh, B., Saha, R., Chandra, A., & Al-Haddad, K. (2009). Static synchronous compensators (STATCOM): a review. IET Power Electronics, 2(4), 297-324.

[8] Richard C.. Dorf, & Bishop, R. H. (2008). Modern control systems. Pearson Prentice Hall.

[9] Duan, G. R., & Yu, H. H. (2013). LMIs in control systems: analysis, design and applications. CRC press.

[10] Lofberg, J. (2004, September). YALMIP: A toolbox for modeling and optimization in MATLAB. In 2004 IEEE international conference on robotics and automation (IEEE Cat. No. 04CH37508) (pp. 284-289). IEEE.

[11] ApS, M. (2019). Mosek optimization toolbox for matlab. User's Guide and Reference Manual, Version, 4.

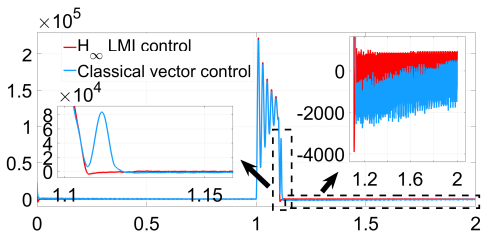

Fig. 8. Reactive power flow to grid from PCC (Var)

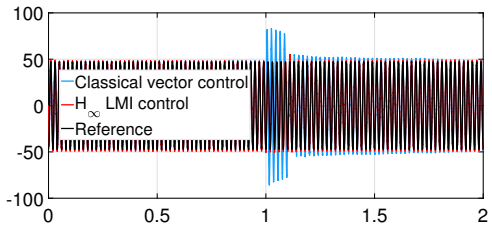

Fig. 9. Phase A AC VSC terminal current (A)

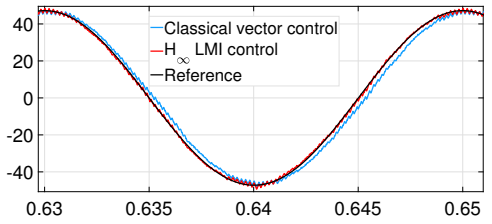

Fig. 10. Phase A AC VSC terminal current (A) - 1st zoom-in

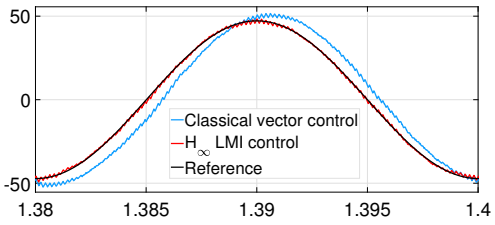

Fig. 11. Phase A AC VSC terminal current (A) - 2nd zoom-in

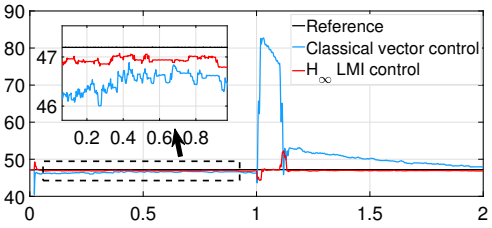

Fig. 12. Phase A AC VSC terminal current (A) in RMS

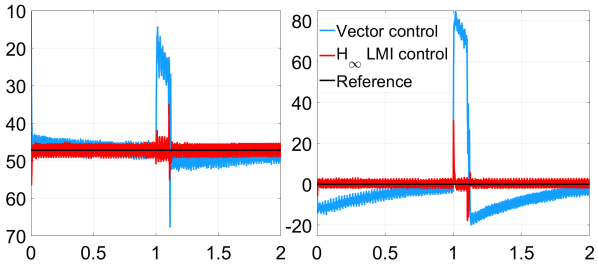

Fig. 13. Current I_d (left) and I_q (right) in dq frame (A)